Fast and reliable non-linear heterogeneous FE approach for the analysis of FRP-reinforced masonry arches

Elisa Bertolesi [a], Gabriele Milani [a,*], Roberto Fedele [b]

[a] Department of Architecture, Built Environment and Construction Engineering (ABC), Politecnico di Milano, Piazza Leonardo da Vinci 32, 20133 Milano, Italy
[b] Department of Civil and Environmental Engineering (DICA), Politecnico di Milano, Piazza Leonardo da Vinci 32, 20133 Milano, Italy

A simple and reliable finite element model is presented, specifically conceived for the analysis of FRP-reinforced masonry arches. The approach proposed relies on the reduction of mortar joints to interfaces exhibiting a non-linear holonomic behaviour under mixed mode conditions, whilst bricks are discretized by means of four-noded elements remaining linearly elastic up to failure. The FRP re-inforcements glued at the intrados or at the extrados are modelled by means of truss bar 2-node el-ements connecting contiguous nodes of the discretized support, with elastic-brittle behaviour in tension and no strength in compression. The predictions provided by the plane stress model, exploiting also the Italian CNR Recommendations for the engineering practice, are validated against some recent experimental results concerning circular and parabolic masonry arches reinforced by glass and carbon FRP.

Keywords:
A. Fibres
A. Carbon fibre
C. Finite element analysis (FEA)
C. Numerical analysis
Masonry arches

1. Introduction

The mechanical assessment of masonry arches beyond elasticity is a classic topic in computational mechanics, that however so far has been tackled almost exclusively in the framework of limit analysis [1–7]. As a matter of fact, limit analysis in the form of both lower and upper bound theorems allows for a direct estimation of the load carrying capacity of the structure without expensive step-by-step simulations. Especially in the study of masonry arches with plastic hinges, to which the assumption of no tension materials well adapts, limit analysis admits also graphical solutions: in those cases both thrust lines (static approach) and the four hinges mechanism (kinematic approach) can be provided. There are however some major limitations in the application of conventional limit analysis, intrinsically linked to its basic hypotheses, as for instance the perfectly plastic behaviour of the material (damage or post-peak soft-ening response are therefore excluded), the unlimited ductility and the plastic flow associativity. Especially this latter assumption seems to adapt with difficulty to all those phe-nomena involving bricks sliding along the mortar joints, which represent preferential planes of weakness for the arches. Moreover, the assumption of unlimited ductility does not allow for estimating displacements at collapse, circumstance which makes limit analysis unsuitable for common displacement based design. Even when, to simulate real engineering structures, the material is assumed scarcely or not resistant at all in tension and with a limited compressive strength, conventional limit analysis has shown to work effectively, mainly because flexural hinges with plasticization in both tension and compression is an associated phenomenon, see e.g. Heyman [2–4] and Oppenheim [5]. Nowadays modern and efficient computerized models [6,7] have superseeded at hand calculations, but limit analysis in the form of either the static or the kinematic the-orem continues being extremely utilized in the engineering community.

The problem becomes however more complex in case of reinforcement by FRP strips. In the last 25 years, several re-searchers were attracted by the prospective of using FRP ma-terials for the retrofitting of r.c. and masonry structures in general, see Refs. [8–11] for an historical perspective. In the literature, several studies are available dealing with this topic

* Corresponding author.
E-*mail address:* gabriele.milani@polimi.it (G. Milani).

Published Journal Article available at: http://dx.doi.org/10.1016/j.compositesb.2015.11.005

(the reader is referred for instance to few sampled papers [12–14] among many), because such innovative technique is becoming very popular in common rehabilitation of monumental and historical buildings, due to the reduced invasiveness and high performance at failure.

Such kind of strengthening essentially acts transferring tensile stresses from masonry (unable to withstand them) to the FRP reinforcement, which typically is extremely resistant under normal positive actions. As a consequence, their utilization for the seismic upgrading or simple rehabilitation of masonry arches became immediately interesting and a variety of experimental results and numerical models (mainly basing on limit analysis or assuming for the materials a brittle behaviour) are nowadays available in the technical literature, see Refs. [15–35].

The key issue in any kind of strengthening remains however the debonding of the FRP strips from the support [36–45], usually referred to as delamination. As well known, delamina-tion is a quasi-brittle phenomenon, which can be characterized at the macroscale through a post-peak decrease of the rein-forcement bearing capacity, as outlined for instance in the recent Italian guidelines on r.c./masonry external reinforcement with composite materials [46]. On the basis of experimental evi-dences gathered so far, it can be stated that the introduction of FRP strips tends to prevent the formation of flexural hinges at the reinforced locations, diffuses damage from mortar joints (concentrated hinge) to neighbouring bricks and potentially ac-tivates sliding phenomena between contiguous bricks, which usually do no occur in unreinforced arches. General agreement exists on the fact that, with respect to the unreinforced case, the collapse of reinforced arches occurs at significantly larger ver-tical deflection and according to a failure mechanism in which the formation sequence and the location of plastic hinges may be altered.

To confront these important issues, a heterogeneous finite element model is proposed in this paper and put at disposal for the engineering practice. In order to accurately assess the predictive capabilities of the proposed model and at the same time validate the design formulae recently proposed by the Italian CNR Recommendations [46], several experiments on FRP reinforced arches have been considered for a critical comparison.

The paper is organized as follows. Section 2 outlines the test configurations adopted in the experimental campaigns mentioned above, together with the main experimental results. The mathematical model proposed to describe the arches response is outlined in Section 3, and design formulae are dis-cussed to calibrate the governing parameters. Section 4 is devoted to an assessment of numerical predictions at the light of experi-mental data. Closing remarks and future prospects are included in Section 5.

Notation. Vector notation is adopted everywhere. Acronyms LVDT and FE indicate Linear Variable Differential Transducer, apt to measure a relative displacement component among assigned points, and Finite Elements Method. Fibre Reinforced Polymers are indicated by the acronym FRP, specifying when necessary those constituted of Carbon (CFRP) or Glass (GFRP) fibres. For the reader's convenience, a table is also provided, including main symbols and abbreviations.

Notation table	
RE	University of Minho externally reinforced arches
RI	University of Minho internally reinforced arches
UR	University of Minho unreinforced arches
CER	University of Padua CFRP externally reinforced arches
GER	University of Padua GFRP externally reinforced arches
$\boldsymbol{B}_S$	Compatibility matrix including rotated shape functions
$\boldsymbol{U} = [\,\boldsymbol{U}^+ \quad \boldsymbol{U}^-\,]^T$	Partitioned vector of interface nodal displacements (+positive surface of the joint, - negative surface of the joint)
$\|J\|$	Jacobian of the interface element
$F_{\text{int}}^{(e)}$	Interface internal forces vector
$K_u^{(e)}$	Element tangent stiffness matrix
$\boldsymbol{K}_{\mathbf{u}}$	Constitutive tangent stiffness at the Gauss point
$\boldsymbol{\Delta}$ (Δ_n, Δ_t)	Interface displacement jump, including normal and tangential components
$\boldsymbol{T} = [\sigma(\boldsymbol{\Delta})\tau(\boldsymbol{\Delta})]^T$	Interface vector stress, including normal and tangential stress components as a function of displacement jumps
c	Mortar cohesion
ϕ	Mortar friction angle
ϕ_n (ϕ_t)	work of separation under pure Mode I (Mode II)
δ_n (δ_t)	pure Mode I (Mode II) characteristic lengths.

2. Reference experimental data

In this study, laboratory experiments on two typologies of arches reinforced with FRP strips were considered as a methodological reference, namely: (a) circular arches tested at the University of Minho [23,45]; (b) parabolic arches tested at the University of Padua [15]. An outline of these experiments is reported in what follows, whereas for further details the interested reader is forwarded to Refs. [15,23].

(a) Circular arches of University of Minho

Arches with semi-circular shape constituted of in scale (1:2) bricks were tested at University of Minho, both UnReinforced (labelled as UR) and Reinforced, for the latter the entire Reinforcement being glued at the Extrados (ER) or at the Intrados (IR), see Ref. [23]. These arches (labelled in what follows as UMinho), with in plane thickness equal to 50 mm, had a free span L = 1500 mm and an out-of-plane width equal to 450 mm. Mortar joints were 10 mm thick.

Two replicates per typology were tested up to failure, under increasing vertical loading applied at one fourth of the span. Several LVDTs monitored the arch deformation, also at the springing. Two continuous GFRP strips, each one 50 mm wide (and therefore not covering the entire out-of-plane width), were glued at the Extrados (RE) or at the Intrados for RE and RI typologies, respectively. Overall experimental responses in terms of applied load F and underlying vertical deflection δ are shown in Fig. 1. As it can be noticed, the unreinforced arches showed a rather brittle failure at about 1.5 kN, with a limited ductility (1–2 mm deflection). Both samples collapsed for a four hinge mechanism. The application of the reinforcement caused a significant increase of both the maximum loading and ultimate displacements. For the arches Reinforced by FRP sheets at the Intrados (labelled as RI) or at the Extrados (labelled as RE), collapse mechanism involved four plastic hinges, two at the lateral supports, one at the left near the applied load and another one symmetrically located on the right. A detachment of the strips was lately observed. Intuitively, the presence in a given section of a reinforcement from the side of tensile stresses prevents the plastic hinges from being activated in that location.

(b) Parabolic arches at University of Padua

Another series of parabolic arches, with span L = 2000 mm and out-of-plane width 1000 mm, were reinforced by FRP sheets and subjected to laboratory tests at University of Padua (Italy) [15]. The arches (labelled in what follows as UniPD) were constituted of real-scale bricks arranged in a single skin, with in plane thickness 55 mm, see Fig. 2. The arch directrix followed the shape of a cate-nary curve, with the appearance of a depressed arch. Two different types of fibres, carbon and glass, where applied at the extrados of the vaults (two replicates of each type), thus a comparison with UMinho tests in (a) can concern exclusively the RE configurations. Reinforcement was constituted of two strips of laminate, also in this case not covering the entire out-of-plane width. In order to obtain similar increments in strength, the overall surface of the strips was equal to 70 mm for carbon and 200 mm for glass, which possesses a lower stiffness. An increasing loading was generated through two hydraulic jacks and applied at one fourth of the span by means of a steel beam, up to activate a failure mechanism. Experimental load–displacement curves are shown in Fig. 2. Un-fortunately, data for the unreinforced configuration were not pro-vided. As it can be observed, in this experimental study the experimental scatter resulted markedly lower with respect to UMinho tests.

3. Finite Element models

To investigate the response of the masonry arches described above, a simple but effective heterogeneous model is proposed herein based on the finite element method. Since the reinforcement does not cover the entire out-of-plane width of the arches, plane-stress conditions are assumed. Some analyses under plane strain conditions were also performed for the considered configurations, which provided negligible differences in the overall response. As well known, “plane strain” conditions imply non-vanishing out-of-plane normal stresses into bricks. On the contrary, constitutive relationships for bidimensional joints usually do not include an explicit dependence on the out-of-plane stress, and therefore they are not sensitive to possible changes in plane stress/plane strain conditions. Indeed these elements should be considered as approximations of the actual 3D behaviour. The same consideration holds a fortiori for the external FRP reinforcements, modelled as uniaxial rods. Consistently with the present purposes of application by not specialized personnel in view of engineering practice, a coarse discretization for the tested arches was adopted, although comparative analyses with refined meshes were performed and discussed in what follows. Each brick was discretized by means of a unique four-node isoparametric element, assumed to behave linearly elastically along the entire loading history. Nonlinear dissipative processes were concentrated along the FRP strips, located at the intrados or extrados of the masonry arches, and into the mortar joints, each covered by a unique interface element as outlined in what follows.

3.1. Interface elements for mortar joints

The mechanical response of mortar joints was described by means of interface elements, including two dominant deformation modes, namely peel (mode I) and shear (mode II) or a combination of two (mixed mode).

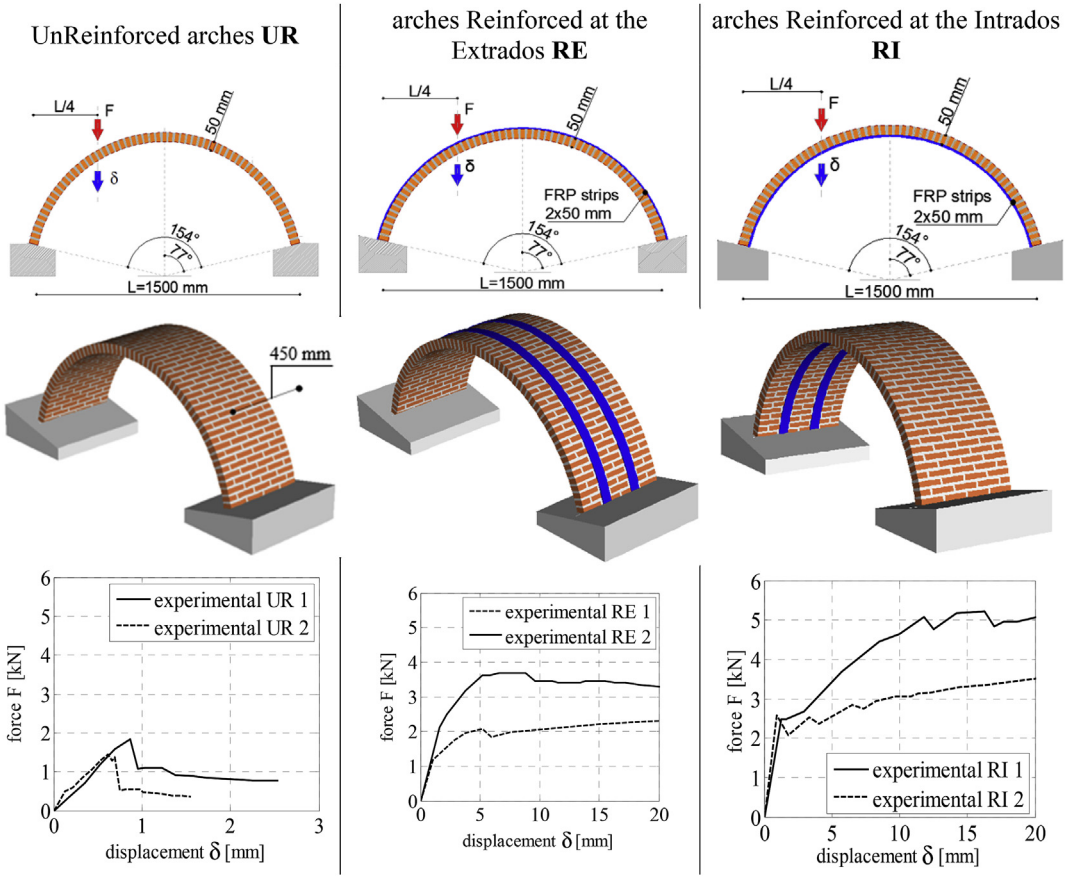

Fig. 1. UMinho circular arches. Geometrical features and overall experimental response.

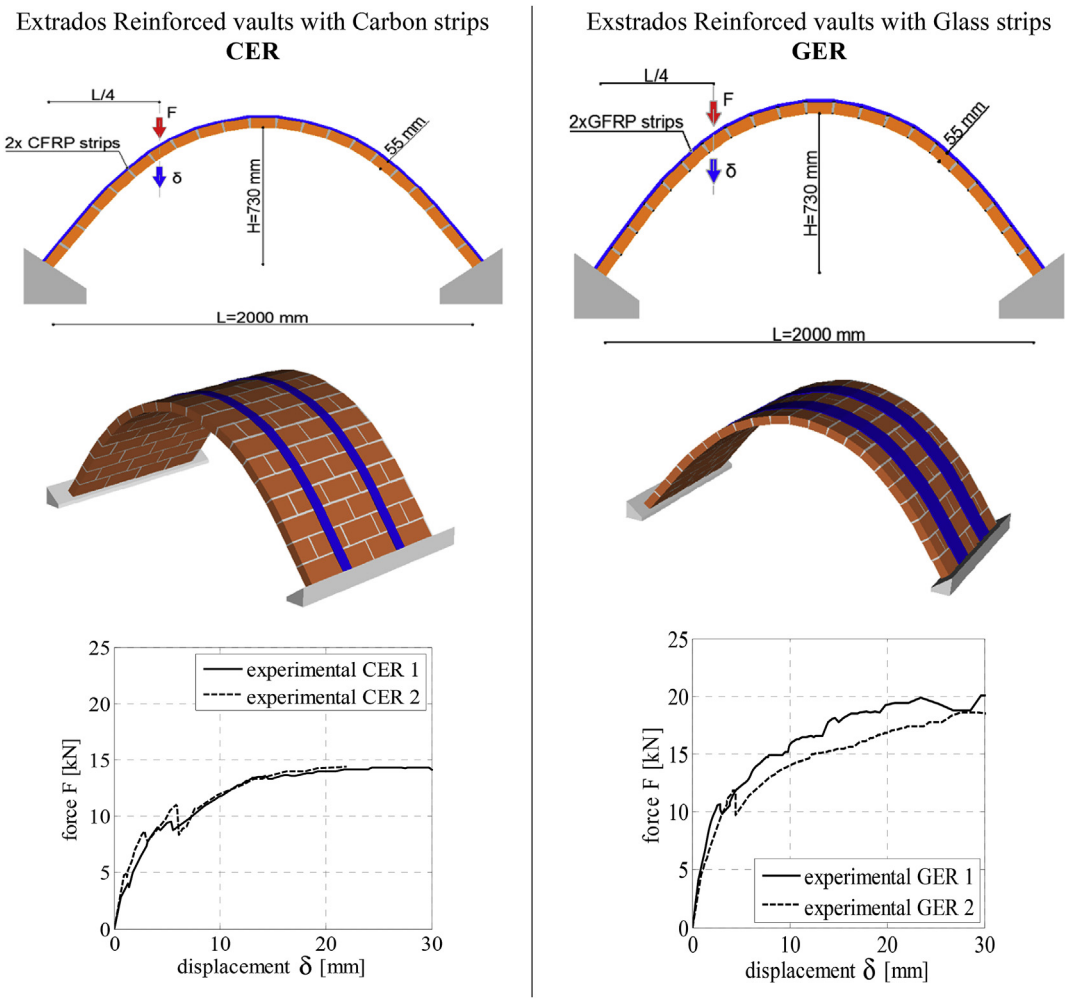

Fig. 2. UniPD parabolic arches. Geometry and experimental load–displacement curves.

Such elements are equipped with a constitutive relationship referred to as "holonomic" since expressed in terms of normal and tangential tractions σ and τ as a path independent function of the normal and tangential relative displacements at the interface, hereafter named respectively Δ_n and Δ_t. Such cohesive relationships are characterized by a post-peak softening branch to be specified in what follows.

In the presence of finite thickness interfaces, relative displacements are evaluated starting from the initial gap between corresponding nodes of two opposite surfaces of the joint, as shown in Fig. 3, indicated by superscripts $+$ and $-$. The vector of the nodal displacement can be partitioned on $\boldsymbol{U} = \left[\boldsymbol{U}^+ \quad \boldsymbol{U}^-\right]^T$ and the relative displacement vector $\boldsymbol{\Delta}$, including normal Δ_n and tangential displacement Δ_t with respect to the joint assumed accordingly as:

$$\Delta = \begin{Bmatrix} \Delta_n \\ \Delta_t \end{Bmatrix} = \left[-\boldsymbol{B}_S\boldsymbol{U}^- \quad \boldsymbol{B}_S\boldsymbol{U}^+\right] = \boldsymbol{B}\boldsymbol{U} \tag{1}$$

where $\boldsymbol{B}_S$ is a suitable compatibility operator, including linear shape function along the (possible rotated) interface abscissa and taking into account finite thickness. The functional dependence of cohesive tractions $T \equiv \{\sigma\ \tau\}^T$ on the relative displacements, dual in the sense of work, $\{\Delta_n \quad \Delta_t\}^T$, will be specified later. Quantities of interest at the (e)-th element are computed as follows: the internal force vector $\boldsymbol{F}_{\text{int}}^{(e)} = \begin{Bmatrix} -\boldsymbol{F}_S \\ +\boldsymbol{F}_S \end{Bmatrix}$, with $\boldsymbol{F}_S = \int_{-1}^{+1} \boldsymbol{B}_S^T \boldsymbol{T} |J| d\xi$; the tangent stiffness matrix $\boldsymbol{K}_u^{(e)} = \begin{bmatrix} \boldsymbol{K}_S & -\boldsymbol{K}_S \\ -\boldsymbol{K}_S & \boldsymbol{K}_S \end{bmatrix}$ being $\boldsymbol{K}_S = \int_{-1}^{+1} \boldsymbol{B}_S^T \boldsymbol{K}_{\mathbf{u}} \boldsymbol{B}_S |J| d\xi$, where $\boldsymbol{K}_{\mathbf{u}}$ is the constitutive tangent stiffness at the Gauss point, $|J|$ is the Jacobian of the line element and ξ is the iso-parametric line abscissa. It is worth noting that internal force vector may be computed solving the integral analytically, so allowing for a discretization with only one interface along the thickness of the arch.

Under mixed-mode loading conditions expected to occur in the mortar joints, three interface relationships, in a sense alternative, have been considered in what follows and comparatively assessed. (a) A piecewise linear cohesive relationship has been considered, labelled as Set I in what follows, first including normal and tangential responses completely independent on each other (decoupled approach), i.e. $\sigma(\Delta_n)$ and $\tau(\Delta_t)$. Although not realistic, this approach is very straight-forward and allows for an impressive stability and rapid convergence of the algorithms. (b) As an alternative, the cohesive relationship at the previous point (a) can be modified to take into account the frictional behaviour among bricks. In this case the peak tangential stress τ_{lim} is assumed to depend on the current stress level at the interface σ by a classic Mohr-Coulomb criterion, namely $\tau_{lim} = -\sigma + c\tan\phi$, where ϕ and c

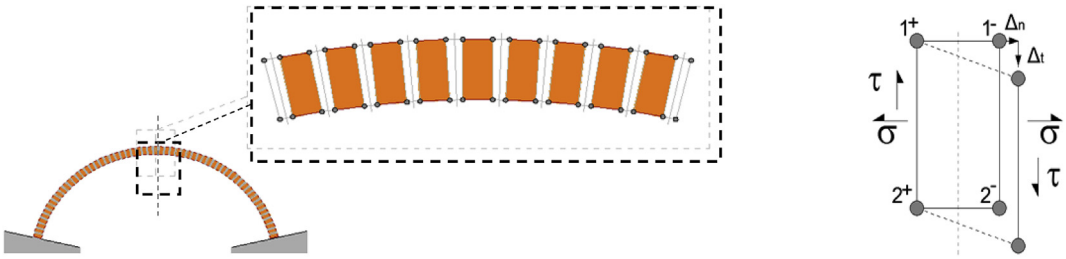

Fig. 3. Interface elements along the arches.

denotes the friction angle and the cohesion, respectively. This choice (labelled as Set III) is intended to describe frictional sliding among the bricks. (c) Finally an improved version of the Xu–Needleman exponential law [47] has been considered, labelled as Set II in what follows. In this law the stress vector $\boldsymbol{T}$ at the interface is given the following closed-form expression:

$$\begin{cases} \sigma = \dfrac{\phi_n}{\delta_n}\left(\dfrac{\Delta_n}{\delta_n}\right)\cdot\exp\left(-\dfrac{\Delta_t^2}{\delta_t^2}\right)\cdot\exp\left(-\dfrac{\Delta_n}{\delta_n}\right) \\ \tau = \dfrac{2\phi_t}{\delta_t}\left(\dfrac{\Delta_t}{\delta_t}\right)\cdot\left(1+\dfrac{\Delta_n}{\delta_n}\right)\cdot\exp\left(-\dfrac{\Delta_t^2}{\delta_t^2}\right)\cdot\exp\left(-\dfrac{\Delta_n}{\delta_n}\right) \end{cases} \quad (2)$$

Symbols ϕ_n and ϕ_t denote the work of separation under pure Mode I (i.e. when $\Delta_t = 0$) and Mode II (i.e. when $\Delta_n = 0$), respectively, while δ_n and δ_t indicate the relevant characteristic lengths. It is worth emphasizing that Equation (2) implies a strongly coupled response: softening occurs for both the tractions although the interface is being stressed along one direction only. In compression the response of mortar joints was assumed to be linear elastic until the interpenetration constraint is activated through a very high stiffness, acting as a penalty factor.

Finally, two remarks are needed. From a conceptual standpoint, interface elements represent a bidimensional schematization of three dimensional phenomena, and usually their constitutive relationships do not include any dependence on the out-of-plane stress and strain. The cohesive relationships for the mortar joints plotted in Fig. 4 were not calibrated to fit the overall experimental plots available, but parameters were selected "a priori" in agreement with data provided in Refs. [15,23], when necessary integrated with values proposed in the recent literature.

For UMinho arches, the mechanical properties of masonry were experimentally assessed through the compressive testing of 10 representative masonry prisms, finding an average compression strength equal to 9.1 MPa and an average elastic modulus of 2040 MPa. Tests performed on eight cylindrical mortar specimens provided an average compressive strength of 7.3 MPa.

For UniPD arches, the mechanical characterization was done by means of compression tests carried out on masonry wallets or bricks and mortar separately. As a consequence, the only data available are the following: masonry mean compression strength equal to 6.00 MPa, brick compression strength f_{cb} = 8.60 MPa, mortar compression strength f_{cm} = 6.00 MPa.

When dealing with constituent materials tensile and shear behaviour, values of tensile strength, cohesion and fracture energy (i.e. inelastic behaviour) have been directly taken from Refs. [23,34] for UMinho arches. Whilst a deep experimental characterization of such data is missing in Ref. [34], it is worth noting that empirical correlations between compression and tension behaviour and literature surveys seem to confirm the correctness of the values adopted. When dealing with UniPD experimentation, only data in compression where available; however, values of peak tensile strength were assumed 2/30 = 0.067 of f_{cm}, again a value in agreement with consolidated literature in the field -which suggests to range between 1/10 and 1/20 of the compression strength- and CNR DT200 specifics [46]. Elastic moduli of bricks were set equal to E_b = 5000 and 8600 MPa for UMinho and UniPD experiments, respectively, while the Poisson ratio amounted to $\nu = 0.2$ in both cases. For UMinho arches, brick modulus value is in agreement with indications provided by Basilio [34]. By means of the application of the well known rule of mixtures applied in combination with mortar Young modulus, it allows for a good approximation of the experimentally obtained masonry elastic modulus. When dealing with UniPD specimens, data were assumed in order to approximate reasonably well the initial stiffness of the experimental force displacement curves, in absence of a detailed investigation available.

The high values of maximum tangential stress observed in Fig. 4 for Set I and II are only a graphical representation of the fact that in practice, for such models, a shear linearly elastic relationship of the interfaces is adopted. Conversely, realistic values of peak tangential strength, following a Mohr-Coulomb law eventually with tension cutoff as in Ref. [20], where the resistance in absence of pre-compression (i.e. cohesion) is roughly equal to masonry tensile strength, are assumed in Set III.

In view of practical applications to the building practice even by not specialized personnel, rather coarse discretizations were adopted for the tested arches, depicted in Figs. 1 and 2, for UMinho and UniPD experiments respectively. The meshes were generated with the commercial code Strand7 and imported in a Matlab® environment for the finite element code, developed by one of the author, see Ref. [47]. The actual thickness of the mortar joints (10 mm) was considered.

3.2. Design approach to reinforcement delamination

While in the last decades experimental and numerical investigations were devoted to delamination of external reinforcement from concrete structures, only in the last few years this topic has been included in the study of masonry structures [33–45]. On the basis of such experimental evidences corroborated by numerical works, a general agreement exists today on the fact that debonding mainly involves failure of the masonry material, and that the response of the reinforcement turns out to be non symmetric. To describe in a simple but effective way delamination of FRP reinforcement from the masonry support, recourse can be made to cohesive interfaces, being the thickness of the adhesive layer negligible at the structural scale. Analogously to what discussed above for the mortar joints, bonding stresses can be expressed as a function of the relative displacements between masonry and FRP sheets. However, the practical use of this model is made complex by the need to specify additional parameters governing the interface response, possibly linking them to the properties of adherent materials.

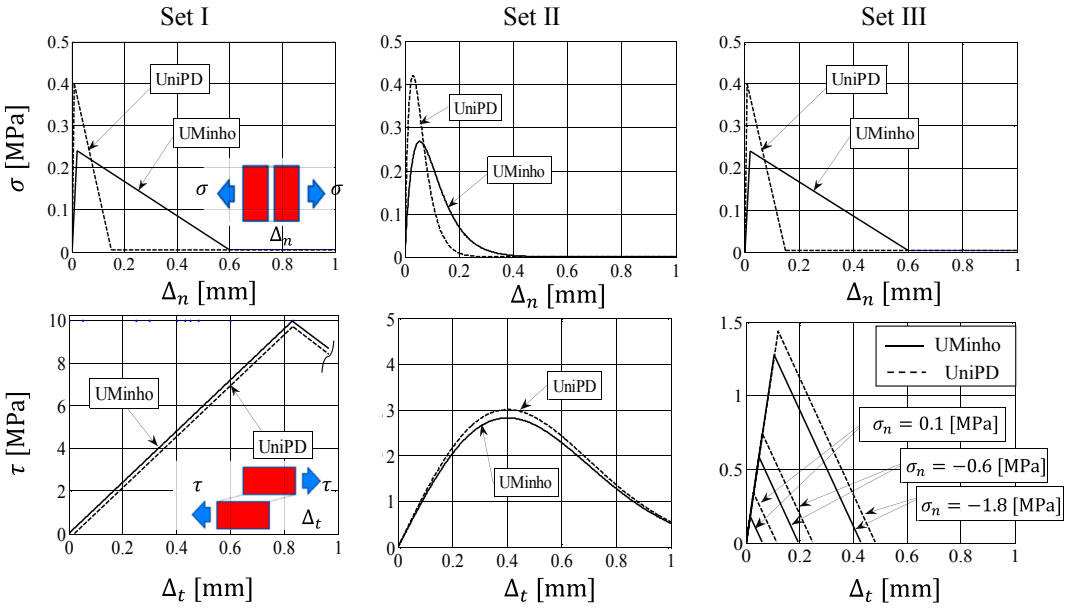

Fig. 4. Normal stress $-\Delta_n$ and tangential stress $-\Delta_t$ relationships assumed for mortar interfaces in the three sets of numerical simulations.

To circumvent such difficulties, in the Italian recommendations CNR-DT200 [46] a simplified formula is proposed to estimate the design bond strength f_{fdd} of FRP elements, namely:

$$f_{fdd} = \frac{1}{\gamma_{f,d}} \sqrt{\frac{2 \cdot E_{FRP} \cdot \Gamma_{Fd}}{t_{FRP}}} \tag{3}$$

where E_{FRP} is the Young modulus of FRP reinforcement (along the main sheet direction), t_{FRP} represents the FRP thickness, $\gamma_{f,d}$ is a safety coefficient specified in the same recommendation [46], herein assumed unitary to simulate ultimate conditions, and Γ_{Fd} is the design specific fracture energy of the masonry support, again provided in Ref. [46]. Equation (3) holds when the bond length l_b exceeds the optimal bond length l_{ed}, condition herein always verified. The optimal bond length can be computed as follows [46]:

$$l_{ed} = \min\left\{ \frac{1}{8\gamma_{Rd}} \sqrt{\frac{\pi^2 \cdot E_{FRP} \cdot t_{FRP}}{2\Gamma_{Fd}}};\quad 150 \text{ mm} \right\} \tag{4}$$

where γ_{Rd} is a heuristic coefficient equal to 1.5 or 1.25 depending on masonry typology.

In this study delamination between FRP and masonry support has been accounted in a simplified manner. The FRP reinforcements were modelled through truss bar 2-node elements connecting contiguous nodes of the discretized support, behaving as an elasto-brittle material in tension and with no strength in compression. Such approach is in agreement to what suggested by the Italian CNR guidelines on RC/masonry reinforcement with composite materials [46], i.e. as elastic-softening rods connecting contiguous nodes, which can break in tension, whilst in compression their strength is assumed to vanish and cannot transmit any force, to properly take into account buckling. Indeed one of the main purposes of this paper was to provide an implicit validation of the above design formulae for engineers. It is well known that under compression FRP sheet may exhibit instability endowed by an early debonding from the substrates. Furthermore, at a structural scale, the accurate modelling of local failure phenomena such as peeling or spalling would require the nonlinear behaviour of the bricks, since FRP debonding mostly occurs for failure of the underlying substrate. However, such phenomena were not observed during the experimental campaign. Tensile peak strength is indeed provided by Equation (3) derived from Italian recommendations mentioned above [46]. The former assumption implies "perfect adhesion" between FRP trusses and the discretized arch, since relative displacements between the adherent materials are completely prevented. This choice significantly simplifies the numerical model and, moreover, it allows to obtain solutions at the macroscale which are in satisfactory agreement with experimental evidences [14].

According to Italian code formulae, characteristic fracture energy is equal to $\Gamma_{Fk} = c_1\sqrt{f_{mk} f_{mtm}}$, where c_1 is a coefficient that, in absence of ad hoc experimental data should be kept equal to 0.015, f_{mk} is the masonry characteristic compressive strength and f_{mtm} is the average masonry tensile strength, which can be assumed according to CNR DT200 [46] equal to 1/10 of masonry characteristic compressive strength.

Taking into consideration design coefficients to pass from characteristic to design values and the values (either adopted or experimental) of masonry compressive strength, the maximum stresses allowable by the FRP reinforcement according to Equation (3) are the following: 75 and 70 MPa for GFRP reinforcement in UMinho and UniPD experiments respectively ($E_{FRP} = 65$ MPa and $t_{FRP} = 0.165$ mm) and 140 MPa for CFRP in ($E_{FRP} = 230{,}000$ MPa and $t_{FRP} = 0.165$ mm) UniPD arches.

Such values are commonly used in design practice, see also [14]. It is worth emphasizing that the numerical exercises which follow should be regarded not only as an assessment of the proposed finite element model, but also as a validation of "a priori" information exploited by the authors for modelling the mortar joint and especially the FRP reinforcement, consistently with Italian CNR DT200 [46], design codes and literature data.

4. Comparative assessment of model predictions

In this section, the numerical predictions provided by the selected models are comparatively assessed on the basis of the experimental data available. It is worth emphasizing that governing parameters for FRP reinforcement and those for mortar joints were

not calibrated by best fitting of the overall experimental data, but "a priori" evaluated according to Italian CNR DT200 [46] and basic information reported by the experimentalists or integrated by literature data.

(a) UMinho circular arches

Overall response of arches in terms of load−displacement curves and deformed arch shapes at collapse provided by the numerical models are shown in Figs. 5−7. In particular, Fig. 5 refers to the un-strengthened (UR) case, Figs. 6 and 7 to the configuration with Reinforcement at the Extrados (RE) and at the Intrados (RI), respectively. In subfigure −a, computed load−displacement plots are compared with the experimental data, whereas subfigure −b shows the magnified deformed shape computed by step-by-step analyses. As a reference, collapse loads are also indicated, predicted by the upper bound Limit Analysis approach developed by one of the authors, see Ref. [20] for further details. Deformed shapes at collapse resulting from different interface relationships for the mortar joints turn out to be coincident. To allow for a comparison among the different configurations, the locations of the hinges along the arches are indicated and labelled by H*i*, where index *i* follows the formation sequence, so that H1 is the first and H4 is the last to be activated under monotonically increasing loading. The actual formation sequence of plastic hinges in the considered UMinho experiments do not corresponds to that predicted by the FE model, whilst a complete agreement is found for the final location. This circumstance is not surprising, for at least two orders of reasons: firstly, the FE model depends on parameters for mortar and FRP reinforcements which were evaluated independently from each other and from the overall response available, and not fitted on it (from this respect they were set "a priori"); secondly, the real constraints turn out to be compliant, on the contrary of the ideal ones, described in the mechanical model.

With reference to the UnReinforced arches (UR) Fig. 5-b, the first hinge is located near the loaded section, implying tensile cracks at the intrados, the second and third at the abutments (left and right) and the fourth hinge opens with cracks at the extrados in a symmetric position with respect to the first hinge. In the real experiments the first hinges resulted located at the springings.

As expected, in Fig. 5-a load−displacement plots provided by Set I and Set III analyses are almost undistinguishable, both based on a piecewise linear cohesive relationship.

This circumstance seems to indicate that flexural hinges are predominant in the failure mechanism without significant sliding between contiguous bricks. The peak load provided by such models is close to the value predicted by Limit Analysis, and to that resulting from the experiments. However the experimental plots exhibits one major drop of loading, followed by a minor one. For the present configuration also Set II simulations, resting on the coupled exponential relationship in Fig. 4, has provided a very similar saw tooth response, which typically encompasses discrete systems with a limited number of mechanisms to be activated.

In the presence of FRP reinforcement, see Figs. 6 and 7, an important increase of ductility can be observed in the experimental response as well as in the model predictions, with vertical deflections one order of magnitude larger with respect to the unreinforced arches. The agreement with the experimental data, which however exhibit a not negligible scatter, has to be regarded as satisfactory for both the configurations. For the arches Reinforced at the Extrados (RE) in Fig. 6, the experimental plots show slight oscillations during the loading phase and a significant scatter. The peak load computed by the numerical models of Sets I and II is approximately equal to the average of those provided by laboratory tests, whilst Set III turns out to be more close to one of the two experimental replicates. All simulations turn out to underestimate the initial stiffness resulting from the experiments and the peak load provided by Limit Analysis. After the peak, the model pre-dictions exhibit a sequence of two sudden drops of loading whose experimental counterpart can only be qualitatively envisaged. Also for this configuration the three interface relationships led to predict the same four hinge mechanism, shown in Fig. 6-b. It is worth emphasizing that a little but perceivable sliding of the bricks was predicted near H4 hinge, in a part of the arch where the external reinforcement tends to prevent the joints from opening.

With reference to the arches Reinforced at the Intrados (RI) in Fig. 7, mechanical models predict a slightly lower initial stiffness with respect to the experimental data, reaches soon a peak load which is very close to that estimated by Limit Analysis and is attained by only one experimental replicate but at a much larger deflection whilst the second experimental replicate remains far from it. After the peak, numerical plots exhibit a sequence of three sudden drops followed by a slow hardening, and at increasing deflection they turn out to underestimate the residual load bearing capacity resulting from the laboratory tests. In particular, at increasing deflection Set I and Set III remain close to one experimental replicate, Set II after having shown an intermediate response diverges from both the experimental data and the plots provided by other Sets of simulations. In all cases predictions provided by the FE models result in safety favour.

As a general trend common to both the reinforced configurations (RE and RI), hinges are less pronounced with respect to the

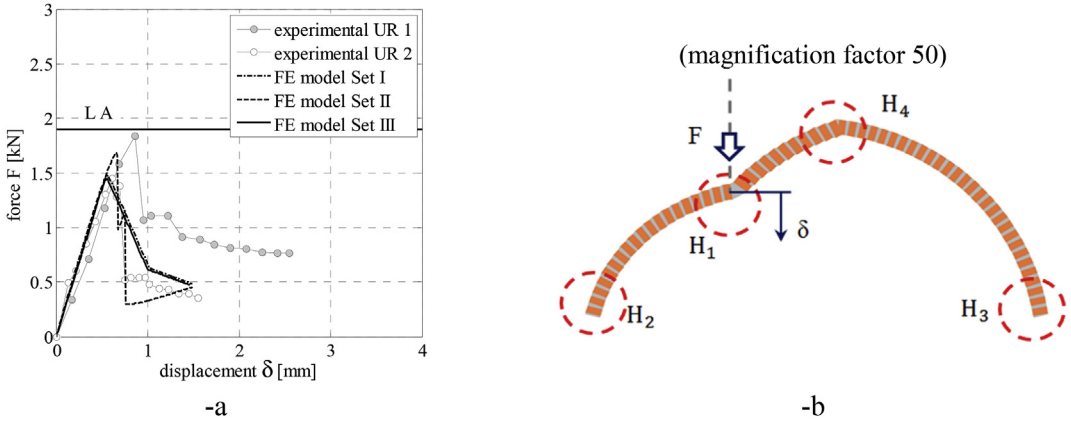

Fig. 5. UMinho UR arch. −a: load displacement curves. −b: four hinges mechanism found numerically.

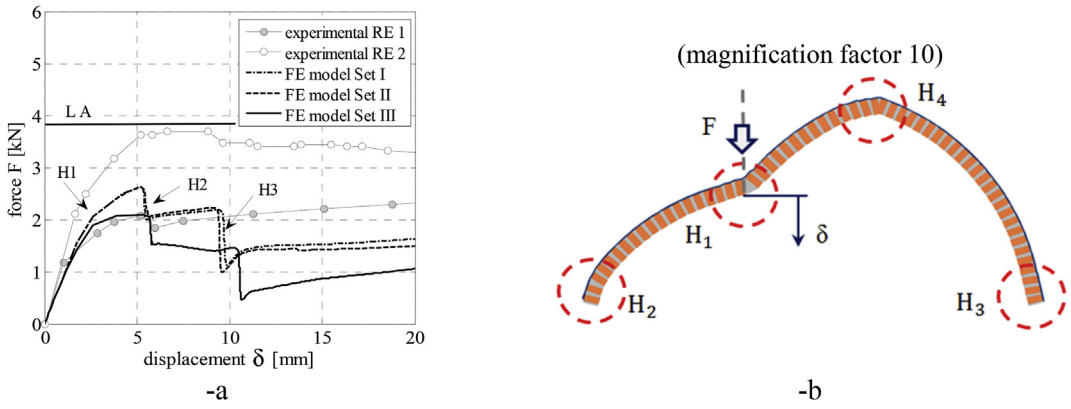

Fig. 6. UMinho RE arch. –a: load displacement curves. –b: four hinges mechanism found numerically.

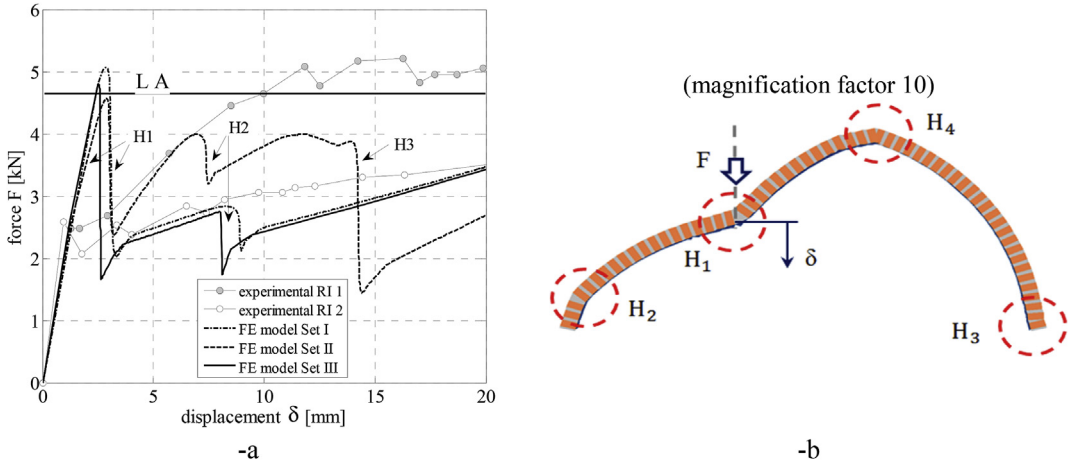

Fig. 7. UMinho RI arch. –a: load displacement curves. –b: four hinges mechanism found numerically.

unreinforced situation (UR) and damage spreads involving several contiguous mortar joints.

Finally, in order to have a more clear understanding of the differences in magnitude of the expected and predicted values, in Table 1 few numeric values meaningful for engineers (peak load, deflection at peak and elastic stiffness), are synoptically reported for the three arches analysed (UR, RE and RI).

Table 1
UMinho arches. Synopsys of some meaningful characteristics of the load displacement curves.

	Peak load [kN]	Elastic stiffness [KN/mm]	Deflection at peak [mm]
UR arch			
Experimental	1.8	2.11	0.85
Set I	1.5	2.72	0.55
Set II	1.7	2.61	0.65
Set III	1.45	2.68	0.54
RE arch			
Experimental	3.7	1.46	5
Set I	2.7	0.91	5.4
Set II	2.7	0.91	5.5
Set III	2.2	0.82	5.5
RI arch			
Experimental	5.2	2.6	14
Set I	5	2	2.5
Set II	4.6	1.70	2.7
Set III	4.8	1.92	2.5

In the Authors' opinion, a reasonable agreement among model predictions and experimental data is found in all cases inspected, considering also the simplifications introduced in the model proposed. It is worth emphasizing that experimental data shown a wide scatter and only two replicates are at disposal. In Fig. 6, model predictions till to peak load are generally "centered" with respect to experimental values, but soon after they exhibit a few sudden drops, becoming far and far from the experimental data.

Unfortunately, a clear description of the activated failure mechanism with detailed *post-mortem* photo documentation is not available to the authors. Oliveira and co-workers report in Ref. [23] that UR arch fails for the formation of a classic four hinges mechanism, quite similar to that found with the present numerical model. RE arches exhibit three flexural hinges and a shear sliding of the support is observed in correspondence of the right abutment. If the FRP strip is assumed perfectly bonded and well anchored to the support (as in the case numerically analyzed) such a failure cannot be reproduced, because FRP is modelled by means of equivalent truss elements perfectly connected node by node to the support. An approach with interface elements allowing for normal out-of-plane debonding (spalling) would be required to reproduce the local detachment of the reinforcement. A similar remark can be repeated for RI, where a local detachment of the strip is observed near the point of application of the external load, late during the experimental test. In this latter case, however, the formation of the four flexural hinges is more evident and reasonably similar to the

experimental one, with damage spreading on larger areas near the central hinge, as correctly reproduced.

The presence of sudden drops of the force displacement curve may be related to (i) the adopted coarse discretization (a unique quadrilateral element for each brick and a unique interface element for each mortar joint), (ii) the material behaviour assumed for bricks and mortar, and (iii) to the mortar/FRP interface law adopted for the reinforced arches, simplistically considered by means of the utili-zation of perfectly bonded brittle trusses, as envisaged in the Italian CNR DT200 [46]. In Fig. 7 the main discrepancies concern the peak load, which for the model was attained soon after the elastic branch, whilst only progressively reached by the experimented samples, and the sudden drops of the force displacement curve, leading to model predictions progressively far (but not too much) from the experi-mental data. Also in this case the experimental scatter between two different experimental replicates is negligible at the beginning but increases considerably with the deflection. One could question why numerical experimental discrepancies are mainly located at large deflections for RE data (Fig. 6), and at the beginning of the overall response, soon after the peak, for RI data (Fig. 7). Reasonably, the experimental response for RI arches includes crushing and compressive behaviour for the mortar joint at the first hinge, which cannot be captured by the model. Moreover, other approximations can be related to the way the external force is applied at the extrados, necessarily constrained by the adopted discretization.

(b) Parabolic arches

With reference to the second experimental campaign (labelled as UniPD), overall plots and computed deformed shapes at collapse are depicted in Fig. 8 for the unreinforced case, in Fig. 10 for the Carbon fibre Extrados Reinforcement (CER) and in Fig. 11 for the Glass Extrados Reinforcement (GER). It is worth mentioning that, to allow for a comparison of the relevant bearing capacities, Valluzzi and co-workers [15] selected as reinforcement wider strips of glass fibres, which are less stiff and resistant than carbon ones. For these experiments information on formation sequence of plastic hinges were not provided.

Since experimental data for unreinforced configuration were not available, Fig. 8 shows exclusively model predictions. In Fig. 8 overall plots by Set I and Set III simulations, with piecewise linear laws uncoupled and frictionally coupled respectively, are almost coinci-dent: this circumstance seems to indicate the absence of significant sliding between contiguous bricks, also as a consequence of different brick geometry (1:1 scale) and of a different arch profile. Coupled relationship of Set II exhibits indeed a marked saw tooth response including a sequence of four marked sudden drops (or three, if we neglect last one, less pronounced). The global appear-ance of the response remains quasi brittle, whilst the deformation scenario is well predicted by all the interface relationships.

Comparative analyses, see Fig. 9, were performed with two refined meshes (hereafter labelled as Mesh 2 and Mesh 3, with two and four elements along the thickness respectively) assuming Set II mechanical properties for joints. It can be observed that, when the number of elements along the thickness is increased, the peak load tends to slightly decrease and the behaviour in correspondence of the hinges formation results smoother. These circumstances indicate that such “spurious” drops were partly due to the presence of only one interface element through the arch thickness. The residual strength for large deflection tends to decrease, again in agreement with intuition, but does not vanish due to the infinitely elastic behaviour in compression of the arch.

Despite such limitations, the Authors consider the adoption of a coarse mesh crucial to favour the effective applicability of the model by practitioners equipped with simple laptops.

The application of the reinforcing strips over the parabolic arches has the twofold effect of increasing the ultimate ductility of the structure as well as the load carrying capacity, as shown in Figs. 10 and 11. The exponential law (Set II) fits accurately the experimental data as well as the uncoupled interface relationship (Set I), whereas Set III (bilinear law with Mohr-Coulomb coupling) progressively deviates from the experimental plots, exhibiting a markedly lower load carrying capacity although endowed by a similar ductility.

Similarly to UMinho case, only few images of the active failure mechanisms are available in Ref. [15]. From a detailed analysis of data reported in Ref. [15], it can be however stated that common features are present, as sliding of the bricks in correspondence of the right abutment and a diffusion of damage near H4 hinge, in correspondence of the FRP at the extrados. As already pointed out, brick sliding is hardily reproducible in the numerical model, because trusses representing the FRP are perfectly bonded to the support, even if some inelastic shear deformation near the right abutment is in any case visible from the deformed shape. Conversely, the diffusion of damage near the central hinge is reasonably simulated, despite the fact that the assumption of elastic bricks makes such diffusion less intuitively evident, since inelastic dissipation can occur only on contiguous mortar joints.

This circumstance can be due to the capability of Sets I and II of describing brick sliding, clearly visible at collapse for both reinforced configurations in between H1 and H3 hinges (see Figs. 10 and 11). On the contrary, since higher axial forces are expected in the reinforced parabolic arches, brick sliding is prevented by frictional coupling, which generates an extremely high tangential strength at the mortar joints. On the basis of the numerical exercises above discussed, the decoupled piecewise linear relationship for the mortar joints exhibits the best predictive capabilities as for the structural response of the arches, with and without reinforcement, and a quite promising convergence rate. The coupled exponential law provided equally accurate predictions, but as a serious drawback it exhibited also marked drops of loading in the overall response without a clear physical meaning, plus a larger computational cost, Table 2, due to the possible shear softening.

Finally, analogously to what done for UMinho arches, in Table 3 experimental peak loads, deflections at peak and elastic stiffnesses, are synoptically compared with their computed counterparts. In general, the agreement of two models (Set I and Set II) over three should be considered very satisfactory. The residual discrepancies at increasing deflection could be linked to the governing parameters adopted for both mortar joints and FRP reinforcement, not calibrated to fit the experimental plot but evaluated from the design formulae proposed in the Italian CNR DT200 [46]. In all cases, the numerical predictions are always below the experimental counterparts, and therefore should be considered to be in safety favour. It is worth emphasizing that for UniPD arches not only the overall geometry but also the utilized bricks and mortar joints had different sizes with respect to UMinho ones. The better agreement observed here could be also derived from the mode of application of the load, in this case more realistically described by the mathe-matical model.

5. Closing remarks and future prospects

In this paper a 2D heterogeneous finite element model has been presented, to simulate the response of masonry arches reinforced with FRP sheets, glued at the intrados or at the extrados.

The plane stress discretization of the selected arches was extremely simple: each brick was modelled by a unique quadrilateral element, behaving linearly elastically even in compression; each mortar joint was described by a unique interface element

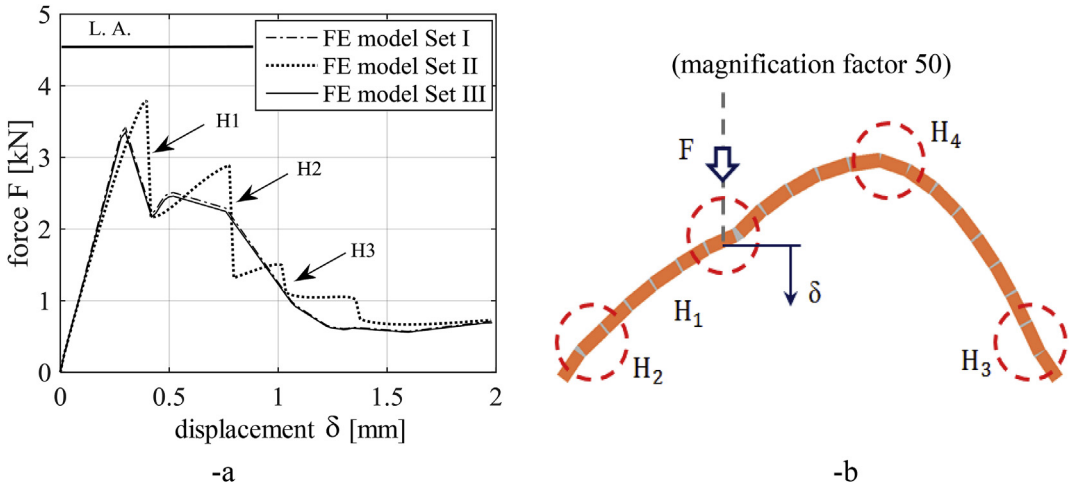

Fig. 8. UniPD unreinforced arch. –a: load displacement curves. –b: four hinges mechanism found numerically.

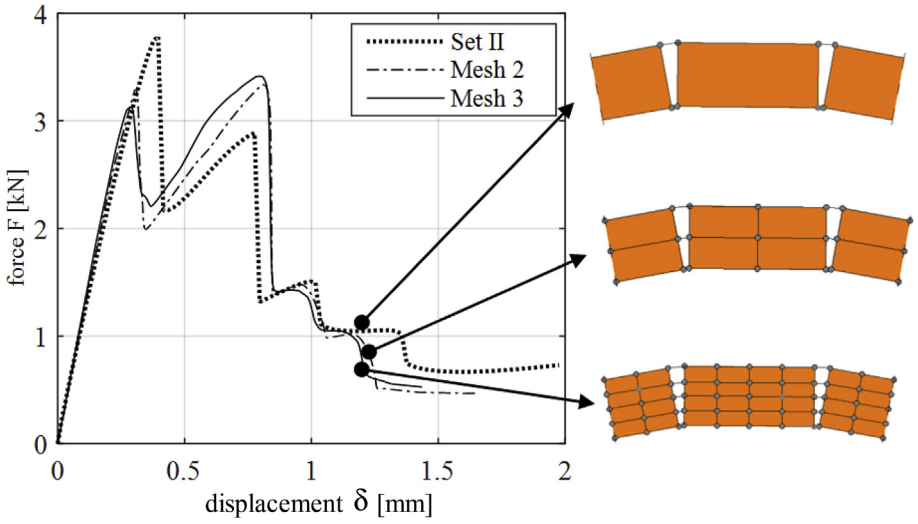

Fig. 9. UniPD unreinforced arch. Mesh dependence study assuming Set II mechanical properties for the joints.

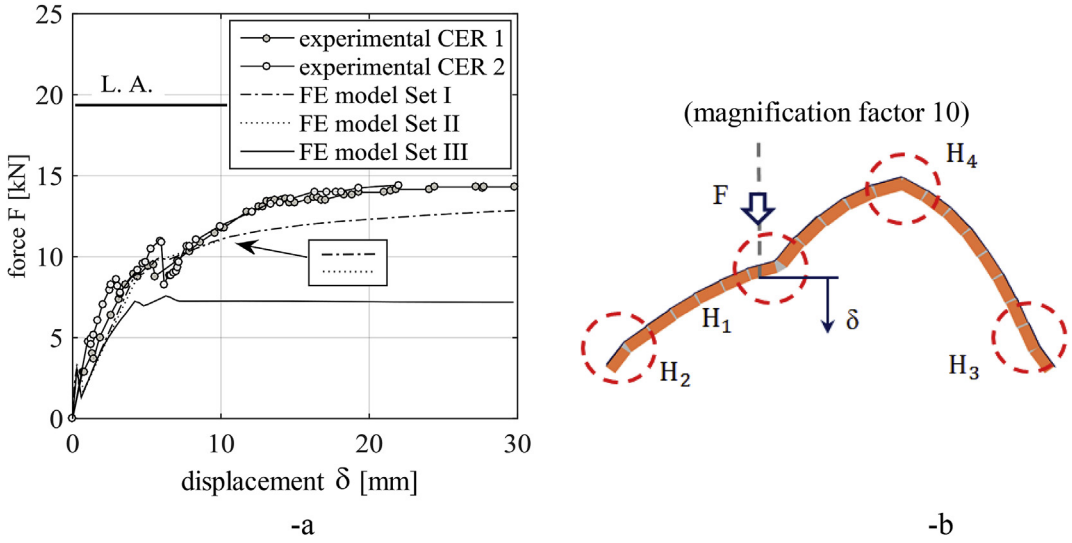

Fig. 10. UniPD CER arch (i.e. with Carbon fibre reinforcement at the extrados). –a: load displacement curves. –b: four hinges mechanism found numerically.

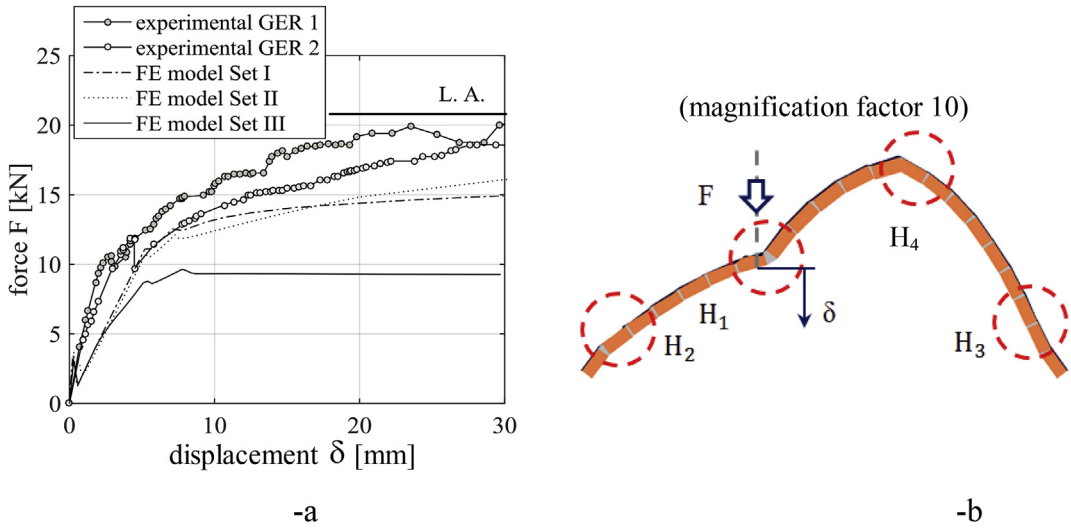

Fig. 11. UniPD GER arch (i.e. with Glass fibre reinforcement at the extrados). −a: load displacement curves. −b: four hinges mechanism found numerically.

Table 2
Synopsis of processing times needed in the different examples to solve the problems investigated (in minutes: seconds).

	UR	RE	RI	Unreinforced	CER	GER
Set I	21:21	39:51	41:01	5:32	7:01	9:09
Set II	44:58	51:06	54:33	12:44	15:02	14:11
Set III	36:25	48:03	55:12	7:01	11:27	12:37

• Results obtained on a Laptop Equipped with MS Win 7 64 bit, 16 Gb RAM.
• Results refer to FE models with one element along the thickness.

Table 3
UniPD arches. Synopsys of some meaningful characteristics of the load displacement curves.

	Peak load [kN]	Elastic stiffness [KN/mm]	Deflection at peak [mm]
CER arch			
Experimental	14	3	18
Set I	9	2.6	5
Set II	9	2.6	5
Set III	8.5	2.8	6.5
GER arch			
Experimental	19	4	19
Set I	12	4	8
Set II	12	4.1	8
Set III	9.8	4.2	7.7

through the arch thickness, equipped with suitable cohesive relationships in tension and no strength in compression. In particular, three sets of holonomic cohesive relationships for mortar interfaces subjected to mixed mode loading conditions were comparatively assessed on the basis of experimental data, assuming either a piecewise-linear (decoupled or frictionally coupled, in Set I and Set III respectively) or a coupled exponential shape (Set II). Parameters of such relationships were not fitted on the overall response, but derived "a priori" on the basis of a few properties of constituents available or from literature data. FRP reinforcing strips were modelled as truss bar 2-node elements connecting contiguous nodes at the intrados or extrados of the discretized masonry surfaces. Their behaviour was assumed elastic brittle in tension, while no strength was assumed in compression.

Two cases of technical relevance, relying into reinforced arches with a circular and parabolic profile and different brick geometry, experimentally tested at the University of Minho [23] and Padua [15], have been critically analysed to benchmark the model proposed and also the design formulae utilized to evaluate the FRP reinforcement parameters. All the cohesive relationships selected for the mortar joints led to satisfactory results in both the reinforced and unreinforced configurations: among them, special emphasis should be attributed to the decoupled piecewise linear law, for both its simplicity and rapid convergence.

It is interesting to notice that the approach proposed exhibits excellent numerical stability, thanks to the reduced number of elements used -one along the thickness- and the total strain formulation adopted (typical of holonomic models), especially in presence of localized strain softening on forming hinges. This is the reason why fragile phenomena with strain softening concentration (as it occurs when strain localizes in the first hinge) may be reproduced with relative easiness, as well as the drop of load bearing capacity after the crack opening, immediately after the activation of any hinge.

Whilst the computational cost of such step-by step simulations is still markedly higher than that required by limit analysis, much more information on the behaviour of the reinforced and unreinforced arches up to failure are at disposal for design purposes, such as formation sequence of the hinges, failure of the FRP strips, softening branches in the overall plots etc. The sequence of plastic hinges reported only for UMinho experiments was not reproduced by the numerical simulations, although the final hinge location was the same.

As future developments, computational provisions are under study to improve the description of local delamination phenomena with bulk dissipation inside the masonry support, see e.g. Refs. [33−45]. Such provisions together with improved design formulae for the reinforcement and mortar joints are expected to decrease the unresolved residuals observed between numerical predictions and experimental plots especially at large deflections. Moreover, Digital Image Correlation procedures are under study, to accurately monitor in situ the deformation scenario over the arches at different observation scales. Kinematic full-field measurement thus available will be synergistically combined with finite element models for an effective identification of governing parameters (see Refs. [45,47]).

References

[1] Kooharian A. Limit analysis of voussoir (segmental) and concrete arches. J Am Concr Inst 1952;49(12):317−28.

[2] Heyman J. The safety of masonry arches. Int J Mech Sci 1969;43:209–24.
[3] Heyman J. Equilibrium of shell structures. Oxford: Oxford University Press; 1977.
[4] Heyman J. The masonry arch. Chicester: Ellis Horwood; 1982.
[5] Oppenheim IJ. The masonry arch as a four-link mechanism under base motion. Earthq Eng Struct Dyn 1992;21(11):1005–17.
[6] O'Dwyer D. Funicular analysis of masonry vaults. Comput Struct 1999;73(1–5):187–97.
[7] Milani E, Milani G, Tralli A. Limit analysis of masonry vaults by means of curved shell finite elements and homogenization. Int J Solids Struct 2008;45(20):5258–88.
[8] Saadmantesh H. Fiber composites of new and existing structures. ACI Struct J 1991;91(3):346–54.
[9] Eshani MR. Strengthening of earthquake damaged masonry structures with composite materials. In: Proc: nonmetallic (FRP) reinforcement for concrete structures. Proceedings of the second international RILEM symposium FRPRCS-2; 1997. p. 681–7.
[10] Triantafillou TC. Composites: a new possibility for the shear strengthening of concrete, masonry and wood. Compos Sci Technol 1998;58:1285–95.
[11] Triantafillou TC. A new generation of composite materials as alternative to fiber reinforced polymers for strengthening and seismic retrofitting of structures. In: Nicolais L, Meo M, Milella E, editors. Proc: Composite Materials. A vision for the future. Springer-Verlag London Limited; 2011.
[12] Corradi M, Borri A, Vignoli A. Strengthening techniques tested on masonry structures struck by the Umbria–Marche earthquake of 1997–1998. Constr Build Mater 2002;16(4):229–39.
[13] Marcari G, Manfredi G, Prota A, Pecce M. In-plane shear performance of masonry panels strengthened with FRP. Compos Part B Eng 2007;38:887–901.
[14] Grande E, Milani G, Sacco E. Modelling and analysis of FRP-strengthened masonry panels. Eng Struct 2008;30(7):1842–60.
[15] Valluzzi MR, Valdemarca M, Modena C. Behavior of brick masonry vaults strengthened by FRP laminates. J Compos Constr ASCE 2001:163–9.
[16] Foraboschi P. Strengthening of masonry arches with fiber-reinforced polymer strips. J Compos Constr 2004;8:191–202.
[17] Baratta A, Corbi O. Stress analysis of masonry vaults and static efficacy of FRP repairs. Int J Solids Struct 2007;44:8028–56.
[18] Briccoli Bati S, Rovero L. Towards a methodology for estimating strength and collapse mechanism in masonry arches strengthened with fibre reinforced polymer applied on external surfaces. Mater Struct Mater Constr 2008;41: 1291–306.
[19] Marfia S, Ricamato M, Sacco E. Stress analysis of reinforced masonry arches. Int J Comput Methods Eng Sci Mech 2008;9:77–90.
[20] Milani G, Milani E, Tralli A. Upper bound limit analysis model for FRP-reinforced masonry curved structures. Part II: structural analyses. Comput Struct 2009;87:1534–58.
[21] Elmalich D, Rabinovitch O. Stress analysis of monolithic circular arches strengthened with composite materials. J Compos Constr 2009;13:431–41.
[22] Elmalich D, Rabinovitch O. Masonry and monolithic circular arches strengthened with composite materials - a finite element model. Comput Struct 2009;87:521–33.
[23] Oliveira DV, Basilio I, Lourenço PB. Experimental behaviour of FRP strengthened masonry arches. J Compos Constr 2010;14:312–22.
[24] Cancelliere I, Imbimbo M, Sacco E. Experimental tests and numerical modeling of reinforced masonry arches. Eng Struct 2010;32:776–92.
[25] Borri A, Castori G, Corradi M. Intrados strengthening of brick masonry arches with composites materials. Compos Part B Eng 2011;42(5):1164–72.
[26] Caporale A, Luciano R. Limit analysis of masonry arches with finite compressive strength and externally bonded reinforcement. Compos Part B Eng 2012;43:3131–45.
[27] Caporale A, Feo L, Luciano R. Limit analysis of FRP strengthened masonry arches via nonlinear and linear programming. Compos Part B Eng 2012;43:439–46.
[28] Caporale A, Feo L, Luciano R, Penna R. Numerical collapse load of multi-span masonry arch structures with FRP reinforcement. Compos Part B Eng 2013;54: 71–84.
[29] De Lorenzis L, Dimitri R, La Tegola A. Reduction of the lateral thrust of masonry arches and vaults with FRP composites. Constr Build Mater 2007;21: 1415–30.
[30] Drosopoulos GA, Stavroulakis GE, Massalas CV. FRP reinforcement of stone arch bridges: unilateral contact models and limit analysis. Compos Part B Eng 2007;38:144–51.
[31] Rovero L, Focacci F, Stipo G. Structural behavior of arch models strengthened using fiber-reinforced polymer strips of different lengths. J Compos Constr 2013;17:249–58.
[32] Briccoli Bati S, Fagone M, Rotunno T. Lower bound limit analysis of masonry arches with CFRP reinforcements: a numerical method. J Compos Constr 2013;17:543–53.
[33] Basilio I, Fedele R, Lourenço PB, Milani G. Assessment of curved FRP-reinforced masonry prisms: experiments and modeling. Constr Build Mater 2014;51C:492–505.
[34] Basilio I. Strengthening of arched masonry structures with composites materials. Ph.D. thesis, Universidade do Minho www.civil.uminho.pt/masonry.
[35] Basilio I, Fedele R, Lourenço P, Milani G. Numerical and experimental analysis of full scale arches reinforced with GFRP materials. Key Eng Mater 2015;624: 502–9.
[36] Ascione L, Feo L. Modeling of composite/concrete interface of RC beams strengthened with composite laminates. Compos Part B Eng 2000;31(6–7): 535–40.
[37] Ascione L, Feo L, Fraternali F. Load carrying capacity of 2D FRP/strengthened masonry structures. Compos Part B Eng 2005;36(8):619–26.
[38] Camli US, Binici B. Strength of carbon fiber reinforced polymers bonded to concrete and masonry. Constr Build Mater 2007;21:1431–46.
[39] Ascione F. Ultimate behaviour of adhesively bonded FRP lap joints. Compos Part B Eng 2009;40:107–15.
[40] Silva MAG, Biscaia HC. Effects of exposure to saline humidity on bond between GFRP and concrete. Compos Struct 2010;93(1):216–24.
[41] Luccioni B, Rougier VC. Shear behaviour of brick–mortar interface in CFRP retrofitted or repaired masonry. Int J Mech Sci 2010;52:602–11.
[42] Fedele R, Milani G. A numerical insight into the response of masonry reinforced by FRP strips. The case of perfect adhesion. Compos Struct 2010;92: 2345–57.
[43] Fedele R, Milani G. Three-dimensional effects induced by FRP-from-masonry delamination. Compos Struct 2011;93(7):1819–31.
[44] Fedele R, Milani G. Assessment of bonding stresses between FRP and masonry pillars during delamination tests. Compos Part B Eng 2012;43(4):1999–2011.
[45] Fedele R, Scaioni M, Barazzetti L, Rosati G, Biolzi L. Delamination tests on CFRP-reinforced masonry pillars: optical monitoring and mechanical modelling. Cem Concr Compos 2014;45:243–54.
[46] CNR-DT200. Guide for the design and construction of externally bonded FRP systems for strengthening existing structures. Italy: C.N.R., National Reaserch Council; March 2012. Revision 8.
[47] Fedele R. Simultaneous assessment of mechanical properties and boundary conditions based on digital image correlation. Exp Mech 2015;55(1):139–53.